arXiv:2201.12939v1 [cs.LG] 27 Jan 2022

Race Driver Evaluation at a Driving Simulator using a physical Model and a Machine Learning Approach*

Julian von Schleinitz[1,*], Thomas Schwarzhuber[1], Lukas Wörle[1], Michael Graf[2], Arno Eichberger[3], Wolfgang Trutschnig[4], Andreas Schröder[4]

Abstract

Professional race drivers are still superior to automated systems at controlling a vehicle at its dynamic limit. Gaining insight into race drivers' vehicle handling process might lead to further development in the areas of automated driving systems. We present a method to study and evaluate race drivers on a driver-in-the-loop simulator by analysing tire grip potential exploitation. Given initial data from a simulator run, two optimiser based on physical models maximise the horizontal vehicle acceleration or the tire forces, respectively. An overall performance score, a vehicle-trajectory score and a handling score are introduced to evaluate drivers. Our method is thereby completely track independent and can be used from one single corner up to a large data set. We apply the proposed method to a motorsport data set containing over 1200 laps from seven professional race drivers and two amateur drivers whose lap times are $10 - 20\%$ slower. The difference to the professional drivers comes mainly from their inferior handling skills and not their choice of driving line. A downside of the presented method for certain applications is an extensive computation time. Therefore, we propose a Long-short-term memory (LSTM) neural network to estimate the driver evaluation scores. We show that the neural network is accurate and robust with a root-mean-square error between $2 - 5\%$ and can replace the optimisation based method. The time for processing the data set considered in this work is reduced from 68 hours to 12 seconds, making the neural network suitable for real-time application.

Keywords: Driver behaviour, Driver-vehicle systems, Driving simulator, Handling, Tire dynamics, High speed

1. Introduction

With the advance of autonomous driving, self-driving cars will continue to encounter emergency situations [1]. In these situations the vehicle has to be controlled at its

*This work was generously supported by BMW AG.
*Corresponding author
[1]BMW AG
[2]Graf Engineering
[3]Technical University of Graz
[4]University of Salzburg

dynamic limit. A task at which most road car drivers are not trained at and lack the required experience. Expert race drivers in contrast exploit the vehicles capabilities to a much greater extent. Gaining insight in race drivers' vehicle handling process might therefore lead to further development in the areas of automated driving, e.g. in case of critical scenarios at the vehicle's dynamic limit. Data from motorsport applications are ideally suited for that task since both engineers and race drivers spend a considerable amount of time on optimising the driver-vehicle system. However, most effort is put into developing the vehicle and not into analysing drivers.
The aim of this work is to provide evaluation methods for drivers which allow general, track independent conclusions on the driving style and point out areas for performance improvement. The best conditions for analysing driving styles provides a driver-in-the-loop simulator since all parameters and circumstances are exactly known at every time step and the simulated environment guarantees reproducible conditions. We develop our method to evaluate race drivers based on the BMW Motorsport simulator which has been in use since 2017. Great effort has been put into matching the simulator with reality, which is the foundation of this work to analyse the performance of race drivers.

1.1. Background

The overall performance in motorsport is the result of driver-vehicle interaction. On a race track, overall performance is usually determined by the lap time. Given a desired trajectory around a race track, the lap time is minimised by maximising the average velocity. Two factors limit maximising the velocity. First, the vehicle can be restrained by the power of the engine to accelerate further. This is called 'power limited'. Second, there is an acceleration limit for the vehicle due to tire-road friction. Track sections where maximising the velocity would violate this limit are referred to as 'grip limited'. Since the power limitation cannot be overcome by the driver we focus on the grip limited track sections in this work. Along a defined trajectory, a vehicle can either accelerate or decelerate. Deceleration to a lower speed is necessary before grip limited track sections (usually corners) that otherwise would require accelerations above the vehicle's capabilities to stay on the desired trajectory. In order to drive fast for as long as possible these deceleration phases need to be as short as possible and the amount of deceleration needs to be maximal. Thus, it is reasonable for the context of this work to define optimal performance as the maximum absolute horizontal acceleration achievable while retaining the spatial path of the vehicle's trajectory. In other words, for optimal performance the available grip should be completely exploited by the vehicle, it would then always be grip or power limited.
The system driver-vehicle has to be described as a closed-loop system. In order to attempt a separation within this system we divide it into four layers as presented in Figure 1. Desirable would be a division into driver and vehicle related performance to determine specific areas of improvement. The *overall performance* in layer 4, as defined above, results from layer 3 which contains the combined *vehicle-trajectory performance* as well as the *handling performance* to keep the vehicle on this trajectory.
On layer 2 we have the *stabilisation performance* to account for the driver's skills to stabilise the vehicle on a given trajectory and the *vehicle performance* to capture the vehicle's capabilities. Influenced by both driver and vehicle are *trajectory* and *driveability*. The trajectory results naturally from the driver's inputs and the vehicle's reaction. Depending on the vehicle setup different trajectories are more or less time-optimal. Driveability

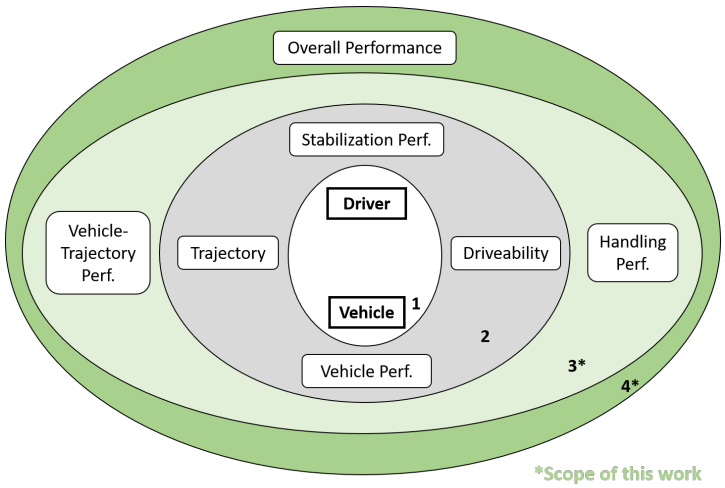


Figure 1: Simplified model to describe how driver and vehicle interactions lead to the overall performance. The driver can choose a trajectory and has a stabilisation performance. The stabilisation performance with driveability lead to the total handling performance. In this work, we present a method to achieve the separation in handling and vehicle/trajectory performance in layer 3.

in the context of motorsport captures how feasible it is for a driver to extract the vehicle's potential. In this work we focus on layer 3 and 4, that is the overall, vehicle-trajectory and handling performance.

1.2. Related work

Donges [2] developed a three level approach of the driving task from an engineering point of view. There are the navigation level, guidance level and stabilisation level. The navigation level includes choosing the appropriate route from a given road infrastructure while also taking an approximate time needed for the route into account. For motorsport application, the course around a race track is predefined, therefore the navigation level is not relevant. The main driving process happens in the guidance and stabilisation level. The guidance level consists of deriving a target trajectory and target velocity, considering the planned driving route and the constantly changing conditions of the track environment. According to the derived targets, control actions are chosen in an anticipatory manner to yield the best possible initial condition with the least deviations from the targets. On the stabilisation level the driver has to manipulate the vehicle controls to keep the deviations to the target trajectory at a minimum level and interacts with the vehicle in a closed loop system. Thereby, the human driver's choice of actions does not solely depend on the current state, but also on prior knowledge and experience according to Macadam [3]. In [4, 5, 6] it is discussed that race drivers have different driving styles while achieving similar lap times. Wörle et al. [4] defined objective criteria for race drivers in professional motorsport, based on their driving control inputs and on their chosen driving trajectories. The algorithm automatically detects cornering manoeuvres and uses pattern recognition to classify different drivers. Similarly, von Schleinitz et al. [7] found that top level race drivers could be distinguished with high accuracy by analysing

only the brake and throttle pedal signals from data of a single corner. Kegelman et al. [6] presented a case study where two professional race drivers employed different driving styles to achieve similar lap times. Accordingly, this supports the idea that driving at the dynamic limit allows a family of solutions in terms of paths and speed. Segers [8] evaluated driving behaviour of race car drivers, by introducing measures based on the performance, smoothness, response and consistency of the driver input signals. The measures were used to objectively detect differences between drivers. Löckel et al. [9] proposed a probabilistic framework for imitating race drivers. They defined a set of metrics based on driver inputs, for example steering or braking aggressiveness to evaluate their framework.
Common motorsport metrics such as lap time, top speed or accelerations provide performance measures but do not give insights how they were achieved nor why certain traits are observed. Also properties which are linked to handling and therefore to driveability are difficult to extract from these metrics [10].
Autonomous race driving is an area where understanding of vehicle handling at the limit is crucial. Kegelman [1] conducted an analysis of data from vintage race cars and quantified the dispersion of paths driven by drivers during races. An autonomous race car is used to research whether the variance observed in human driving is due to error or a consequence of purposefully exploiting the vehicle limits. It showed that expert human drivers operated the vehicle around and also beyond the stability limit on purpose, whereas the autonomous vehicle always remained within the stable region. This way the expert drivers were significantly faster than the autonomous vehicle. Hermansdorfer et al. [11] compared an autonomous software stack to professional human race drivers using common motorsport analysis techniques and came to a similar conclusion. The autonomous software followed the trajectory smoothly but did not drive at the handling limit and was therefore inferior to human drivers. Both studies indicate that a very important talent of race drivers is constantly exploiting the available grip.

However, in reality this is hard to determine since the available grip changes constantly and with it the current dynamic limit of the vehicle. Here, driver-in-the-loop simulators have a big advantage for analysing drivers. de Groot and de Winter [12] studied the effect of training inexperienced race drivers with different levels of grip on a simulator. They measured classical motorsport performance factors such as lap time, full throttle percentage and did questionnaires to assess the drivers confidence. van Leeuwen et al. [13] determined the differences between racing and non-racing drivers on a simulator using eye-tracking. They observed that race drivers showed a more variable gaze behaviour.
Studies about driver evaluation in terms of vehicle handling on a simulator are rare. A possible reason is that motorsport suited simulators are very expensive and motorsport teams usually do not publish their findings. Schwarzhuber et al. [14] introduced the TPER method (tire potential exploitation rating) whereby the difference between the vehicle's acceleration and an optimised acceleration based on a two-track vehicle and a Pacejka tire model is used as an evaluation criteria for different motion cueing algorithms. They investigated steady-state manoeuvres and concluded that TPER is a powerful tool for simulator fidelity investigations.
This work is based on the TPER method, but focuses on driver evaluation instead of simulator development. Therefore, not only steady-state manoeuvres, but complete laps are evaluated. In addition to optimising the vehicle's acceleration, we introduce four optimisers to determine the maximum force on each tire. Comparing the initial state

to these optimised states allows to calculate scores for overall, vehicle-trajectory and handling performance.

1.3. Overview

In chapter 2, the simulator and the vehicle model are detailed and the data set is presented.
Chapter 3 describes the methodology. We optimise the vehicle's acceleration in the center of gravity (Cog) for which we introduce the optCog optimiser and compare it to the initial state. In order to evaluate the performance of the vehicle, a second optimiser which we named optTire evaluates the maximum possible force of each tire independently. In the next step we define scores based on the outcome of the optimiser models that allow differentiation between overall, vehicle-trajectory and handling performance. We also propose a LSTM-based machine learning architecture to directly determine the scores form the initial data.
Chapter 4 presents the results of this study. Having at hand the methods and the data set it is analysed how the drivers exploit the grip by studying the slip ratios and slip angles at the tires and comparing them for the optimization states. We also compare the professional drivers to amateur drivers. Lastly, the prediction performance of the machine learning model is shown. Summarized, the main contributions of this work are:

- A method to evaluate race drivers on a simulator based on tire potential exploitation
- Separation of the overall performance in handling and vehicle-trajectory performance
- Application of the introduced method to a data set from professional race drivers on a top-level motorsport simulator
- Comparison of professional drivers to two amateur drivers
- A machine learning model architecture which can replace the optimization based method while being much faster to compute

2. Apparatus

The experiment to evaluate the methodology as an objective driver analysis tool is carried out at a four degrees of freedom (DOF) driver-in-the-loop simulator (DiLS).

2.1. Driver-in-the-loop simulator

The DiLS used for the study is located in Munich and was designed by BMW Motorsport. Therefore, special focus has been put on its applicability for the motorsport environment. It has been operational since 2017. To this day, it is frequently used for vehicle development and driver training.

The mechanical assembly consists of a static 210° curved screen. The screen surrounds a four DOF motion platform on top of which a mock-up of the corresponding race car's chassis is attached. Three of the motion platform's DOFs are rendering angular velocities: yaw rate $\dot{\psi}$, pitch rate $\dot{\theta}$, and roll rate $\dot{\phi}$. Translational motion is displayed in vertical direction (heave) only by means of the heave acceleration a_z. The range and dynamic

capabilities of each DOF were identified using classical system identification techniques. The motion platform is controlled by a custom motion cueing algorithm (MCA) [14]. In addition to the motion and visualization system, stimuli are provided by means of a static sound system and the steering force feedback. Both provide relevant information about vehicle states, making them vital parts of the DiLS [15, 16]. The steering wheel is directly driven by an electric motor which allows to display up to 24 Nm of steering torque. The torque demand is derived from the tire forces at the front axle and the vehicle's steering geometry.

All the above mentioned systems and their respective characteristics result in a certain simulator fidelity, which was proven to have an impact on driver-vehicle interaction [17]. For the proposed methodology, the race drivers' behaviour is a fundamental part. In the context of driving simulation the term of validity refers to similar driving behaviour between simulator and in the real world driving tasks. An earlier study conducted at the BMW Motorsport DiLS quantitatively identified its validity [18]. Detailed results are not relevant for the present work but should be considered if an extension to real driving tasks is sought.

2.2. Vehicle Model

The vehicle and tire models are described separately as these are fundamental parts not only of the driving simulator but also of the methodology itself. For vehicle dynamics modelling, a custom two track model is implemented similar as described in [19]. The proposed methodology relies on detailed knowledge of the models. It is a mandatory requirement to have all vehicle and tire model parameters available in order to make the methodology feasible. The models' inputs are twofold. Firstly, the driver controls the vehicle via steering wheel including gear-shifter functionality, the accelerator pedal, brake pedal and clutch pedal. Secondly, a terrain server provides road inputs by means of tires' contact patch coordinates. In order to further process contact patch and tire load information to tire forces, the simulation model is equipped with a Pacejka Magic Formula tire model [20]. The parameters of vehicle and tire models are identified individually by means of test bench data. Subsequently, the models are validated using mainly closed loop manoeuvres. Validity in this context is only defined for circuit racing close to the vehicle's maximum capabilities. The model in use was confirmed to provide relative validity, meaning that vehicle setup variations show the same sensitivities in the virtual and the real environment.

For the purpose of driving simulation, all models are required to be realtime executable. Deploying a compiled version of the models to a *Speedgoat* real-time target machine, allows an execution frequency of 2 kHz.

2.3. Data

The basis of this work is a data set from BMW motorsport. It consists of time series signals from a professional motorsport racing series which are obtained from the aforementioned simulator. Figure 2 provides an overview of the data set. It was logged with a sample rate of 100 Hz and there are over 10 million instances. The data were collected in 2020 as a part of race preparation and consist of seven drivers (D1-D7) on four tracks (T1-T4). Additionally, data from two amateur drivers (D8A and D9A) were collected on track T2.

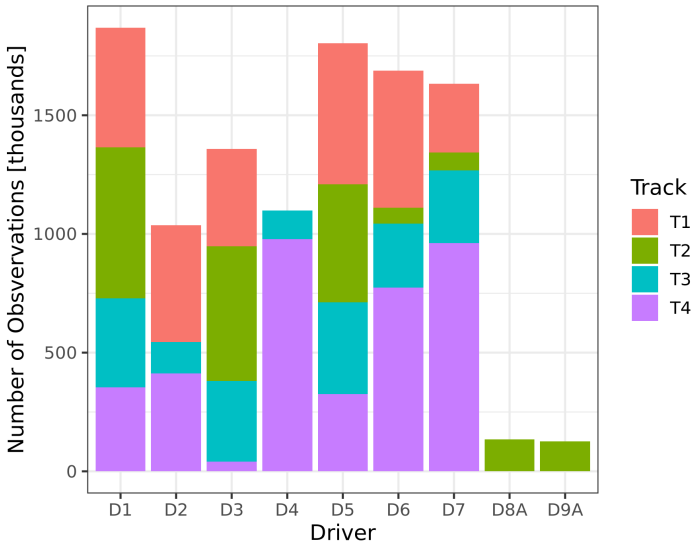


Figure 2: Overview of the data set used in this work. The two amateur drivers D8A and D9A only drove on one race track. In total there are over 10 million observations with a sample rate of 100 Hz.

3. Methods

3.1. Dynamic limit optimisation

The purpose of the method described in this section is to evaluate how far the driver or the vehicle is from the optimum, which is given by the maximum horizontal acceleration while retaining the trajectory or having the highest possible tire forces, respectively. We split the driving task into two parts. According to the three-level model of driving tasks choosing a trajectory corresponds to the guidance level and stabilising the vehicle along this trajectory to the stabilisation level [21, 2].

3.1.1. optCog optimisation

The optCog optimisation is equivalent to the *TPER* method by Schwarzhuber et al. [14], we provide a brief summary of the method in this section. Figure 4a shows a graphical overview. *TPER*, which stands for Tire Potential Exploitation Rating, is based on a two track vehicle model as described in [22] combined with a Pacejka Magic Formula tire model [20]. The vehicle state vector $\dot{\boldsymbol{x}}^{\text{in}}$ is composed according to (1), where the index as with 'a' $\in \{\text{f}, \text{r}\}$ and 's' $\in \{\text{l}, \text{r}\}$ associates the corresponding wheel from front-left to rear-right on the vehicle. For simplicity the vehicle state vector is subdivided into a

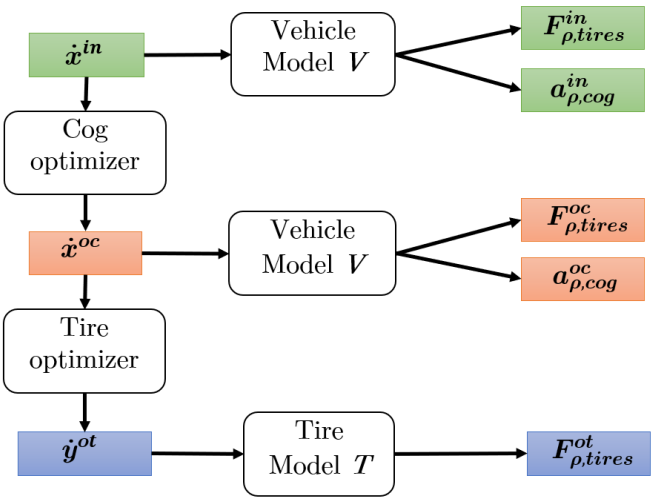


Figure 3: Path from the Init state $\dot{\boldsymbol{x}}^{\text{in}}$ over the optCog state $\dot{\boldsymbol{x}}^{\text{oc}}$ to the optTire state $\dot{\boldsymbol{y}}^{\text{ot}}_{\text{as}}$. Using a vehicle or tire model forces F and accelerations a can be calculated from the state vectors $\dot{x}$ and $\dot{y}$.

constant and a variable part, which changes during optimisation

$$\begin{aligned}\dot{\boldsymbol{x}}^{\text{in}} &= [\dot{\boldsymbol{x}}^{\text{in}}_{const}\ \dot{\boldsymbol{x}}^{\text{in}}_{var}]^{\text{T}},\ \text{with}\\ \dot{\boldsymbol{x}}^{\text{in}}_{const} &= [\dot{\psi}\ v\ Fz_{\text{as}}\ \alpha_{\text{as,n}-1}\ \mu_{\text{as}}\ b_{\text{as}}\ D_{\text{x}}\ D_{\text{y}}\\ &\qquad \gamma_{\text{as}}\ r_{\text{as}}\ n_{\text{Engine}}\ i_{\text{Tot}}\ ],\\ \dot{\boldsymbol{x}}^{\text{in}}_{var} &= [\delta^{\text{in}}\ \beta^{\text{in}}\ \kappa^{\text{in}}_{\text{as}}].\end{aligned} \tag{1}$$

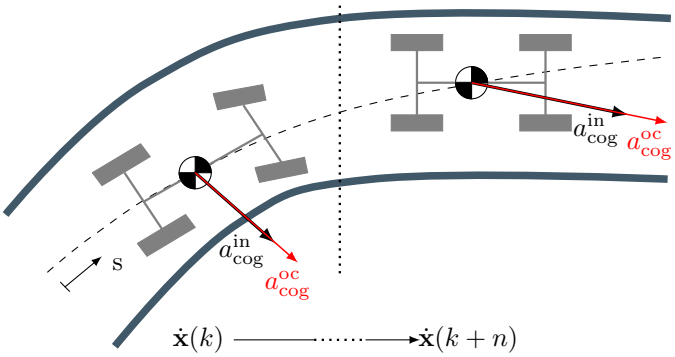
Table 1 provides an overview of the parameters. The aim of the optCog optimisation is to determine an optimised vehicle state vector from $\dot{\boldsymbol{x}}^{\text{in}}$

$$\begin{aligned}\dot{\boldsymbol{x}}^{\text{oc}} &= [\dot{\boldsymbol{x}}^{\text{in}}_{\text{const}}\ \dot{\boldsymbol{x}}^{\text{oc}}_{\text{var}}]^{\text{T}},\\ \text{with } \dot{\boldsymbol{x}}^{\text{oc}}_{\text{var}} &= [\delta^{\text{oc}}\ \beta^{\text{oc}}\ \kappa^{\text{oc}}_{\text{as}}],\\ \text{such that } L^{\text{oc}}(\dot{\boldsymbol{x}}^{\text{oc}}) &= \min L^{\text{oc}}(\dot{\boldsymbol{x}}),\end{aligned} \tag{2}$$

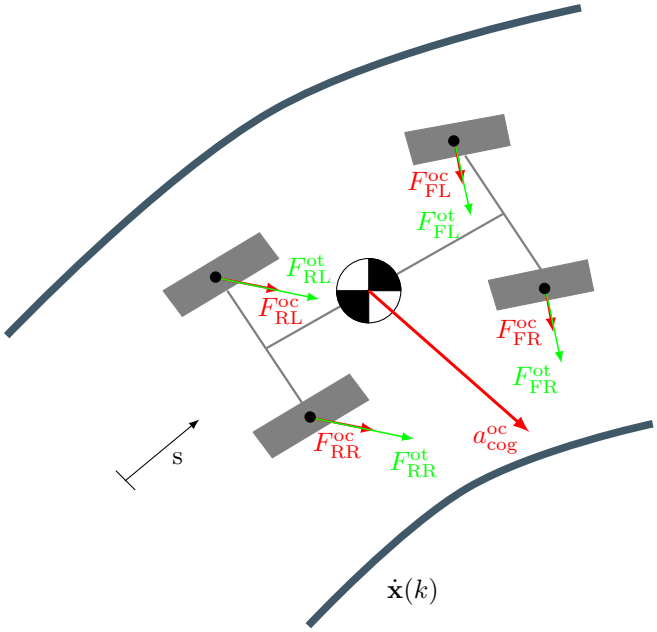
whereby L^{oc} is the loss function and $\dot{\boldsymbol{x}}^{\text{oc}}_{\text{var}}$ are the optimisation variables. In consideration of the external forces $F_{\text{x,ext}}$ and $F_{\text{y,ext}}$, the longitudinal, lateral and angular momentum equalities of the vehicle model are defined.

$$\begin{aligned}m \cdot a_{\text{x,cog}} \ =\ & F_{\text{x,rl}} \cdot \cos\delta_{\text{rl}} + F_{\text{x,rr}} \cdot \cos\delta_{\text{rr}} - F_{\text{y,rl}} \cdot \sin\delta_{\text{rl}} - F_{\text{y,rr}} \cdot \sin\delta_{\text{rr}} +\\ & F_{\text{x,fl}} \cdot \cos\delta_{\text{fl}} + F_{\text{x,fr}} \cdot \cos\delta_{\text{fr}} - F_{\text{y,fl}} \cdot \sin\delta_{\text{fl}} - F_{\text{y,fr}} \cdot \sin\delta_{\text{fr}} +\\ & F_{\text{x,Ext}}\end{aligned} \tag{3}$$

$$\begin{aligned}m \cdot a_{\text{y,cog}} \ =\ & F_{\text{x,rl}} \cdot \sin\delta_{\text{rl}} + F_{\text{x,rr}} \cdot \sin\delta_{\text{rr}} + F_{\text{y,rl}} \cdot \cos\delta_{\text{rl}} + F_{\text{y,rr}} \cdot \cos\delta_{\text{rr}} +\\ & F_{\text{x,fl}} \cdot \sin\delta_{\text{fl}} + F_{\text{x,fr}} \cdot \sin\delta_{\text{fr}} + F_{\text{y,fl}} \cdot \cos\delta_{\text{fl}} + F_{\text{y,fr}} \cdot \cos\delta_{\text{fr}} +\\ & F_{\text{y,Ext}}\end{aligned} \tag{4}$$



a) Visualisation of the optCog optimisation results for two samples. The amount of acceleration in the center of gravity is maximised. The optimisation keeps the initial vehicle trajectory.



b) Qualitative visualisation of the optTire result. The amount of force in each tire is optimised individually. In general, the optimisation does not result in a valid vehicle state nor does it retain the initial trajectory.

Figure 4: Overview of both optimisation methods. They aim at providing a measure of how close the vehicle is to the optimum given the defined constraints.

Table 1: Description of the symbols used in this paper, whereby the index as with 'a' $\in \{\mathrm{f}, \mathrm{r}\}$ and 's' $\in \{\mathrm{l}, \mathrm{r}\}$ associates the corresponding wheel from front-left to rear-right on the vehicle.

Symbol	Description
$\dot{\psi}$	angular velocity around the vertical axis
v	resultant velocity of the vehicle
Fz_{as}	tire loads
$\alpha_{\mathrm{as,n-1}}$	tire slip angles of the previous sample
μ_{as}	dynamic toe angles
b_{as}	half track widths
D_{x}, D_{y}	longitudinal, lateral aerodynamic drag force
γ_{as}	camber angles
r_{as}	dynamic tire radii
n_{Engine}	rotational speed of the engine
i_{Tot}	overall gearing from the engine to the tires
δ	steering angle
β	body sideslip angle
κ_{as}	tires' longitudinal slip ratios
$\dot{\boldsymbol{x}}$	vehicle state vector
$\dot{\boldsymbol{y}}$	tire state vector
$a_{\mathrm{x,cog}}, a_{\mathrm{y,cog}}$	vehilce acceleration the center of gravity
br_{dist}	brake balance
$F_{\mathrm{x,as}}, F_{\mathrm{y,as}}$	forces at the tire contact patch
r_{Throttle}	throttle pedal actuation
r_{Brake}	brake pedal actuation
$r_{\mathrm{Rocker,as}}$	rocker angle (suspension movement)

$$
\begin{aligned}
J_{\mathrm{zz}} \cdot \ddot{\psi} \;=\; & l_{\mathrm{F}} \cdot (F_{\mathrm{x,fl}} \cdot \sin\delta_{\mathrm{fl}} + F_{\mathrm{x,fr}} \cdot \sin\delta_{\mathrm{fr}} + F_{\mathrm{y,fl}} \cdot \cos\delta_{\mathrm{fl}} + F_{\mathrm{y,fr}} \cdot \cos\delta_{\mathrm{fr}}) - \\
& l_{\mathrm{R}} \cdot (F_{\mathrm{x,rl}} \cdot \sin\delta_{\mathrm{rl}} + F_{\mathrm{x,rr}} \cdot \sin\delta_{\mathrm{rr}} + F_{\mathrm{y,rl}} \cdot \cos\delta_{\mathrm{rl}} + F_{\mathrm{y,rr}} \cdot \cos\delta_{\mathrm{rr}}) + \\
& b_{\mathrm{fr}} \cdot (F_{\mathrm{x,fr}} \cdot \cos\delta_{\mathrm{fr}} - F_{\mathrm{y,fr}} \cdot \sin\delta_{\mathrm{fr}}) + \\
& b_{\mathrm{fl}} \cdot (-F_{\mathrm{x,fl}} \cdot \cos\delta_{\mathrm{fl}} + F_{\mathrm{y,fl}} \cdot \sin\delta_{\mathrm{fl}}) + \\
& b_{\mathrm{rr}} \cdot (F_{\mathrm{x,rr}} \cdot \cos\delta_{\mathrm{rr}} - F_{\mathrm{y,rr}} \cdot \sin\delta_{\mathrm{rr}}) + \\
& b_{\mathrm{rl}} \cdot (-F_{\mathrm{x,rl}} \cdot \cos\delta_{\mathrm{rl}} + F_{\mathrm{y,rl}} \cdot \sin\delta_{\mathrm{rl}}) + \\
& M_{\mathrm{z,fl}} + M_{\mathrm{z,fr}} + M_{\mathrm{z,rl}} + M_{\mathrm{z,rr}}
\end{aligned}
\tag{5}
$$

Equations 3 to 5 enable to search for an optimal vehicle state vector $\dot{\boldsymbol{x}}^{\mathrm{oc}}$ in the sense of

$$
L^{\mathrm{oc}}(\dot{\boldsymbol{x}}) \;=\; -\sqrt{(a_{\mathrm{x,cog}})^2 + (a_{\mathrm{y,cog}})^2}. \tag{6}
$$

The objective of the optimisation is to maximise the norm of combined longitudinal ($a_{\mathrm{x,cog}}$) and lateral acceleration ($a_{\mathrm{y,cog}}$). The loss function $L^{\mathrm{oc}}(\dot{\boldsymbol{x}})$ is formulated as a minimisation problem.

For simplicity, the slip ratios are optimised directly, instead of modelling the entire powertrain and braking system. Though, powertrain limitations are formulated as constraints. The first constraint ensures driving trajectory compliance by keeping the

approximated resultant angular acceleration $\ddot{\psi}$ constant

$$\ddot{\psi}^{\mathrm{oc}} - \ddot{\psi}^{\mathrm{in}} \;=\; 0. \tag{7}$$

Furthermore, the direction of the resultant horizontal acceleration has to remain constant

$$\frac{a^{\mathrm{oc}}_{\mathrm{x,cog}}}{a^{\mathrm{oc}}_{\mathrm{y,cog}}} - \frac{a^{\mathrm{in}}_{\mathrm{x,cog}}}{a^{\mathrm{in}}_{\mathrm{y,cog}}} \;=\; 0. \tag{8}$$

Next, constraints for the slip ratios κ_{as} are introduced to consider the dependencies in the vehicle model. The difference in driving and braking torque T_{as} between left and right tire has to remain constant on each axle

$$T^{\mathrm{oc}}_{\mathrm{al}} - T^{\mathrm{oc}}_{\mathrm{ar}} - (T^{\mathrm{in}}_{\mathrm{al}} - T^{\mathrm{in}}_{\mathrm{ar}}) \;=\; 0. \tag{9}$$

Since only rear wheel driven cars are considered, the front axle constraint refers to braking torque only. The initial distribution of braking torques between front and rear axle has to remain unchanged. Therefore, a continuously differentiable braking distribution (br_{dist}) constraint is formulated

$$\begin{aligned} T^{\mathrm{oc}}_{\mathrm{f}} - (T^{\mathrm{oc}}_{\mathrm{f}} + T^{\mathrm{oc}}_{\mathrm{r}}) \cdot br_{\mathrm{dist}} \;&=\; 0, \text{ with} \\ br_{\mathrm{dist}} \;&\approx\; br_{\mathrm{drv}} \cdot \left(\frac{\arctan(-\epsilon_1 \cdot (T^{\mathrm{oc}}_{\mathrm{f}} - \epsilon_2))}{\pi} + \frac{1}{2} \right). \end{aligned} \tag{10}$$

The variable br_{drv} is the constant braking distribution selected by the driver and ϵ_1 and ϵ_2 are small numerical parameters. The range of possible side slip angles and slip ratios is bound to

$$\left(\frac{\alpha^{\mathrm{oc}}_{\mathrm{as}}}{\alpha_{\mathrm{max}}} \right)^2 - 1 \;\leq\; 0, \tag{11}$$

$$\left(\frac{\kappa^{\mathrm{oc}}_{\mathrm{as}}}{\kappa_{\mathrm{max}}} \right)^2 - 1 \;\leq\; 0. \tag{12}$$

Lastly, the maximum driving torque T_{r} is limited to the engine capabilities $T_{\mathrm{Engine_{max}}}$ by

$$T^{\mathrm{oc}}_{\mathrm{r}} - T_{\mathrm{Engine_{max}}} \cdot i_{\mathrm{Tot}} \;\leq\; 0. \tag{13}$$

The optimization is carried out with the *fmincon* solver of the *MathWorks® MATLAB optimization toolbox*. The function *fmincon* finds the minimum of a problem specified by

$$\underset{\dot{\boldsymbol{x}}}{\text{minimize}} \quad L(\dot{\boldsymbol{x}}) \tag{14a}$$

subject to

$$c(\dot{\boldsymbol{x}}) \leq 0 \quad \text{(nonlinear inequalities)}, \tag{14b}$$

$$ceq(\dot{\boldsymbol{x}}) = 0 \quad \text{(nonlinear equations)} \tag{14c}$$

$c(\dot{\boldsymbol{x}})$ and $ceq(\dot{\boldsymbol{x}})$ are functions that return vectors and $L(\dot{\boldsymbol{x}})$ is a function that returns a scalar. $L(\dot{\boldsymbol{x}})$, $c(\dot{\boldsymbol{x}})$ and $ceq(\dot{\boldsymbol{x}})$ can be nonlinear functions [23]. For the problem specified in this work, $ceq(\dot{\boldsymbol{x}})$ contains the vehicle model's momentum equalities (3,4, 5) as well as equality constraints (7,8,9,10). The inequalities contained in $c(\dot{\boldsymbol{x}})$ are described by equations (11,12,13).

3.1.2. optTire optimisation

The optTire optimiser is similar to the optCog optimiser. Instead of the complete vehicle with a state vector $\dot{\boldsymbol{x}}$, every tire state vector $\dot{\boldsymbol{y}}_{\mathrm{as}}$ is optimised independently. Figure 4b visualizes the process. We base the optTire optimisation on the optCog state to make it less dependent on a possibly sub-optimal force distribution from the Init state (this is especially relevant for the amateur drivers). The optCog tire state vector is a subset of the optCog vehicle state vector

$$\dot{\boldsymbol{y}}_{\mathrm{as}}^{\mathrm{oc}} \subseteq \dot{\boldsymbol{x}}^{\mathrm{oc}}. \tag{15}$$

$\dot{\boldsymbol{y}}_{\mathrm{as}}^{\mathrm{oc}}$ is subdivided into a constant part and a variable part, which is altered by the optimiser

$$\begin{aligned} \dot{\boldsymbol{y}}_{\mathrm{as}}^{\mathrm{oc}} &= [\dot{\boldsymbol{y}}_{\mathrm{as,const}}^{\mathrm{oc}}\ \dot{\boldsymbol{y}}_{\mathrm{as,var}}^{\mathrm{oc}}]^{\mathrm{T}}, \\ \dot{\boldsymbol{y}}_{\mathrm{as,const}}^{\mathrm{oc}} &= [\ Fz_{\mathrm{as}}\ \mu_{\mathrm{as}}\ \gamma_{\mathrm{as}}\ r_{\mathrm{as}}], \\ \dot{\boldsymbol{y}}_{\mathrm{as,var}}^{\mathrm{oc}} &= [\alpha_{\mathrm{as}}^{\mathrm{oc}}\ \kappa_{\mathrm{as}}^{\mathrm{oc}}]. \end{aligned} \tag{16}$$

The optTire optimisation results in a new tire state vector

$$\begin{aligned} \dot{\boldsymbol{y}}_{\mathrm{as}}^{\mathrm{ot}} &= [\dot{\boldsymbol{y}}_{\mathrm{as,const}}^{\mathrm{oc}}\ \dot{\boldsymbol{y}}_{\mathrm{as,var}}^{\mathrm{ot}}]^{\mathrm{T}}, \\ \dot{\boldsymbol{y}}_{\mathrm{as,var}}^{\mathrm{ot}} &= [\alpha_{\mathrm{as}}^{\mathrm{ot}}\ \kappa_{\mathrm{as}}^{\mathrm{ot}}], \\ \text{such that } L^{\mathrm{ot}}(\dot{\boldsymbol{y}}_{\mathrm{as}}^{\mathrm{ot}}) &= \min L^{\mathrm{ot}}(\dot{\boldsymbol{y}}_{\mathrm{as}}). \end{aligned} \tag{17}$$

Similar to the vehicle model a tire model $\boldsymbol{T}$ is used to calculate the relevant variables from the tire state vector $\dot{\boldsymbol{y}}$, in this case the forces at each tire in x and y direction

$$F_{\mathrm{as}} = \boldsymbol{T}_{F_{\mathrm{as}}}(\dot{\boldsymbol{y}}). \tag{18}$$

The force generated by each tire is maximised individually

$$L_{\mathrm{as}}^{\mathrm{ot}}(\dot{\boldsymbol{y}}) \ = \ -\sqrt{(F_{\mathrm{x,as}})^2 + (F_{\mathrm{y,as}})^2}, \tag{19}$$

while keeping the direction of the force equal to the optTire state

$$\frac{F_{\mathrm{x,as}}^{\mathrm{ot}}}{F_{\mathrm{y,as}}^{\mathrm{ot}}} - \frac{F_{\mathrm{x,as}}^{\mathrm{oc}}}{F_{\mathrm{y,as}}^{\mathrm{oc}}} \ = \ 0. \tag{20}$$

Note that there does not have to exist a valid vehicle state for the optimised tire state nor a valid trajectory. Similar to the optCog optimiser, the *MathWorks® MATLAB optimisation toolbox* with the *Active-Set* solver option is used.

3.1.3. Scores

As a first step to obtain scores from the optCog results, the acceleration at the center of gravity and forces at the tires in the xy-plane in a polar coordinate system are calculated

$$\begin{aligned} a_{\rho,\mathrm{cog}} &= \sqrt{a_{\mathrm{x,cog}}^2 + a_{\mathrm{y,cog}}^2}, \\ a_{\phi,\mathrm{cog}} &= \mathrm{atan}(\frac{a_{\mathrm{y,cog}}}{a_{\mathrm{x,cog}}}), \\ F_{\rho,\mathrm{as}} &= \sqrt{F_{\mathrm{x,as}}^2 + F_{\mathrm{y,as}}^2}, \\ F_{\phi,\mathrm{as}} &= \mathrm{atan}(\frac{F_{\mathrm{y,as}}}{F_{\mathrm{x,as}}}). \end{aligned} \tag{21}$$

Then, the sum of all tire forces is defined as

$$F_{\rho,\text{tires}} = F_{\rho,\text{fl}} + F_{\rho,\text{fr}} + F_{\rho,\text{rl}} + F_{\rho,\text{rr}}. \tag{22}$$

We define the following metrics which can be interpreted as scores for the system vehicle-driver. The ratio between the amount of initial vehicle acceleration at the center of gravity to the optCog acceleration yields S_{handling}

$$S_{\text{handling}} = \frac{a^{\text{in}}_{\rho,\text{cog}}}{a^{\text{oc}}_{\rho,\text{cog}}}. \tag{23}$$

The vehicle score is defined as the ratio between the optCog and optTire forces

$$S_{\text{veh}-\text{traj}} = \frac{F^{\text{oc}}_{\rho,\text{tires}}}{F^{\text{ot}}_{\rho,\text{tires}}}. \tag{24}$$

Finally, the overall score emerges from the Init forces to the optTire forces

$$S_{\text{tot}} = \frac{F^{\text{in}}_{\rho,\text{tires}}}{F^{\text{ot}}_{\rho,\text{tires}}}. \tag{25}$$

3.1.4. Limitations

Since we apply the optimisation method on a relatively large data set and aim to use the methods for race preparation in future, computation time is a concern. This is also a main reason why we introduce the constraint of a constant driving line which is a simplification since the driver's performance on the stabilisation level also influences the driving line. For example when entering a corner too fast, the vehicle might get pushed towards the outside, although not being intended by the driver. However, for the professional drivers we can assume that they anticipate this effect. This is supported by Macadam [3] who stated that the drivers choice of action is not only based on the current state but also prior knowledge and experience.

We execute the optimisation for approximately 3.5 million data instances. The calculation time for one lap with an average length of 80 seconds is approximately 200 seconds on computer with two 10-core *Intel®Xeon®Silver 4144* CPUs. To reach this speed, both optimiser rely on parallel processing which significantly reduces calculation time. As a consequence, the models compute each data point isolated from its temporal surrounding. Dynamic effects due to changed accelerations from the optimised states are not respected, for example a change in load transfer. However, the closer the Init state is to the dynamic limit (the optCog state) the smaller the error will be, which is where race drivers usually operate the vehicle. Though, for some applications a calculation time of 200 seconds per lap is still too high. For example in race simulations 50 and more laps can be driven and a very quick analysis is needed. The resulting calculation time of 10000 seconds would make it infeasible in practice. Ideal would be a real-time calculation. Therefore, we propose an end-to-end machine learning approach to replace the computational expensive optimisation.

3.2. Machine learning predictor

We propose a machine learning model as an approximation to the aforementioned optimisation approach. Depending on the computer hardware and model size the runtime speed improvement is more than one order of magnitude and the model is real-time application suited. The three scores defined in section 3.1.3 are predicted simultaneously by an artificial neural network $\boldsymbol{P}$ based on $\dot{\boldsymbol{x}}^{\mathrm{p}}$, which is a part of the initial vehicle state vector $\dot{\boldsymbol{x}}^{\mathrm{in}}$

$$[\tilde{S}_{\mathrm{handling}}\ \tilde{S}_{\mathrm{veh-traj}}\ \tilde{S}_{\mathrm{tot}}] = \boldsymbol{P}(\dot{\boldsymbol{x}}^{\mathrm{p}}).$$

3.2.1. Artificial neural network architecture

The model is based on a LSTM neural network architecture, which has been used for time series prediction on a motorsport data set before [24]. The hyperparameters are listed in Table 2 and the architecture in Figure 5. The model is built in R 3.6.2 [25] using the R interface to keras [26] and tensorflow [27].
The LSTM was introduced by Hochreiter and Schmidhuber [28]. A LSTM consists of an *input gate*, *forget gate* and *output gate*. With these, the LSTM can decide which information will be forgotten, learned or passed on to the next time step. The outputs of the previous time step serve as inputs for the current time step. Apart from the output, a LSTM passes a cell state to the next time step. The cell state makes it easier for information to flow unchanged through multiple time steps. This results in the ability of the LSTM cells to learn long-term dependencies while avoiding the vanishing /exploding gradient problem [29, 24].

3.2.2. Data preparation

All time series data are normalized to increase the numerical stability. For this purpose let $\boldsymbol{w} \in \mathbb{R}^m$ be a raw time series signal. Then, $\boldsymbol{x} \in \mathbb{R}^m$ is calculated by

$$\boldsymbol{x} = \frac{1}{\sigma(\boldsymbol{w})}(\boldsymbol{w} - \mu(\boldsymbol{w})\boldsymbol{e}),$$

with the all-ones vector $\boldsymbol{e} \in \mathbb{R}^m$, whereby $\mu(\boldsymbol{w}) \in \mathbb{R}$ is the sample mean and $\sigma(\boldsymbol{w}) \in \mathbb{R}$ the sample standard deviation of $\boldsymbol{w}$.

The data is split in training (80%), validation (10%) and test set (10%). Also, the Track T2 is excluded from the training set to examine the model accuracy on an unseen track.

Table 2: Hyperparameters for the LSTM-based predictor module

Parameter	**Setting**
Learning rate	0.001
Batch size	128
Dropout	0.3
Recurrent dropout	0.1
Optimiser	"Adam" [30]
Input temporal dimension	100
Input feature dimension	24
Output temporal dimension	100
Output feature dimension	3

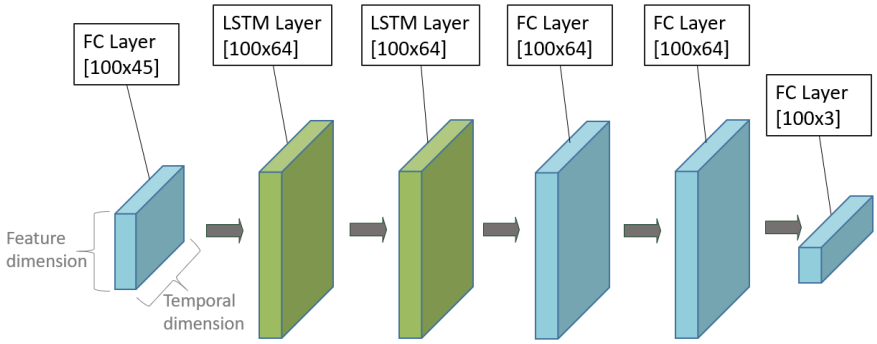


Figure 5: Machine learning predictor model architecture. Two LSTM and two fully connected layers constitute the hidden layers.

3.2.3. Model selection

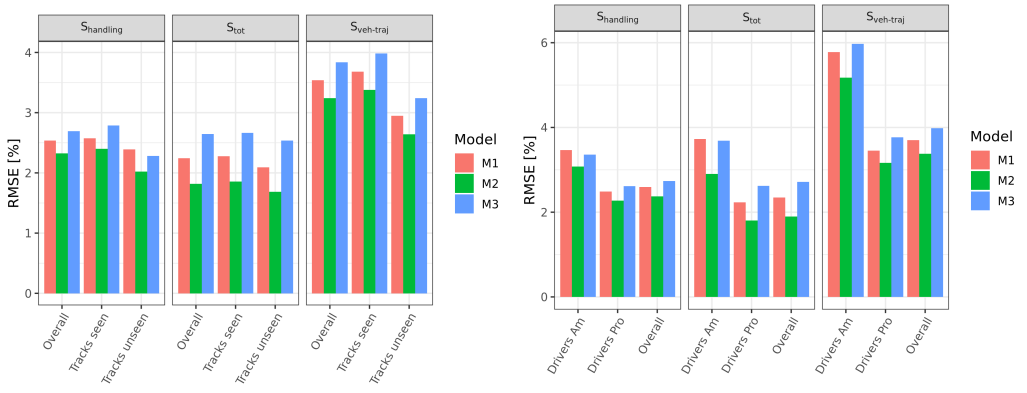
The root-mean square error (RMSE) between prediction and reference is used as an evaluation criteria for the neural network. The RMSE between a reference signal $\boldsymbol{yr}$ and a predicted signal $\boldsymbol{y}$ with m time steps is

$$\mathrm{RMSE}(\boldsymbol{yr}, \boldsymbol{y}) = \sqrt{\frac{1}{m}\sum_{t=0}^{m}(\boldsymbol{yr}^{(t)} - \boldsymbol{y}^{(t)})^2}.$$

Three different models M1, M2 and M3 are trained on the data set. These models have different input time series. All inputs are obtained from the initial vehicle state.

- M1 (32 inputs): α_{as}, κ_{as}, Fx_{as}, Fy_{as}, Fz_{as}, r_{Brake}, r_{Throttle}, $\dot{\psi}$, $a_{\mathrm{x,cog}}$, $a_{\mathrm{y,cog}}$, δ, v, β, $r_{\mathrm{Rocker,as}}$
- M2 (45 inputs): α_{as}, κ_{as}, Fx_{as}, Fy_{as}, Fz_{as}, r_{Brake}, r_{Throttle}, $\dot{\psi}$, $a_{\mathrm{x,cog}}$, $a_{\mathrm{y,cog}}$, δ, v, β, $r_{\mathrm{Rocker,as}}$, γ_{as}, r_{as}, μ_{as}
- M3 (16 inputs): Fz_{as}, r_{Brake}, r_{Throttle}, $\dot{\psi}$, $a_{\mathrm{x,cog}}$, $a_{\mathrm{y,cog}}$, δ, v, β, $r_{\mathrm{Rocker,as}}$

The models' accuracy should be consistent for different factors of influence. Figure 6 shows the RMSE in dependence of tracks as well drivers. To detect possible overfitting to the training data, we compare the RMSE on seen and unseen tracks (which were not a part of the training set) in Figure 6 a. None of the models showed overfitting to the seen tracks, the error on the unseen track is even a bit lower. To further test the models, they are also tested on the amateur drivers' data. The models were only trained on data from the professional drivers, which have distinctly higher scores. The amateur driver scores are therefore well outside the scope of the training data. Figure 6 depicts the resulting RMSE. The error is as expected higher but the models are very usable for the task at hand. This indicates that the models are robust. In all cases the model M2 has the lowest error and is therefore chosen for this work. The additional inputs compared to M1 and M3 contained additional information which helped the model to predict more accurately. Since the advantage of M2 is also visible for unseen tracks and the amateur drivers it is not a result of overfitting.



a) Prediction model accuracy over tracks. The tracks are split into seen tracks, which were part of the training set and unseen tracks which were not. There is no significant RMSE difference between the two cases.

b) Model accuracy over drivers. The professional drivers 'Drivers Pro' were part of the training set, whereas the amateur drivers 'Drivers Am' were not. The error for the amateur drivers is clearly higher, however, still in the same range.

Figure 6: In all cases the model M2 has the lowest error. The error for the prediction of $S_{\text{veh}-\text{traj}}$ is generally higher than for S_{handling} or S_{tot}.

3.3. Control states

In order to analyse driver performance independent from a specific track section, control states are defined based on the driver's inputs. Three boolean variables describe if the brake pedal, throttle pedal or steering wheel angle δ are active

$$B_{brake} = \begin{cases} 1, & \text{if } r_{\text{Brake}} > 10bar \\ 0, & \text{otherwise,} \end{cases} \tag{26}$$

$$B_{throttle} = \begin{cases} 1, & \text{if } r_{\text{Throttle}} > 10\% \\ 0, & \text{otherwise,} \end{cases} \tag{27}$$

$$B_{steer} = \begin{cases} 1, & \text{if } |\delta| > 10° \\ 1, & \text{if } |\dot{\delta}| > 500°/s \\ 0, & \text{otherwise.} \end{cases} \tag{28}$$

The second condition for B_{steer} ensures that occasions where the steering angle is small but the change rate is high, are included. This can be for example during a quick counter steer.
The combination of the boolean variables results in the four control states. These relate to the commonly defined cornering sections [10], which are in parentheses:

- Pure brake (Braking): $B_{brake} = 1,\ B_{throttle} = 0,\ B_{steer} = 0$
- Trail brake (Turn Entry): $B_{brake} = 1,\ B_{throttle} = 0,\ B_{steer} = 1$
- Pure steer (Mid Corner): $B_{brake} = 0,\ B_{throttle} = 0,\ B_{steer} = 1$

- Throttle steer (Turn Exit) : $B_{brake} = 0,\ B_{throttle} = 1,\ B_{steer} = 1$

The other possible combinations are not relevant for the driver analysis in the context of this paper. For example under pure throttle the vehicle's acceleration is usually limited by the engine and not the driver. An overview of the control states in the time domain is e.g. depicted in Figure 7.

4. Results

4.1. optTire optimisation

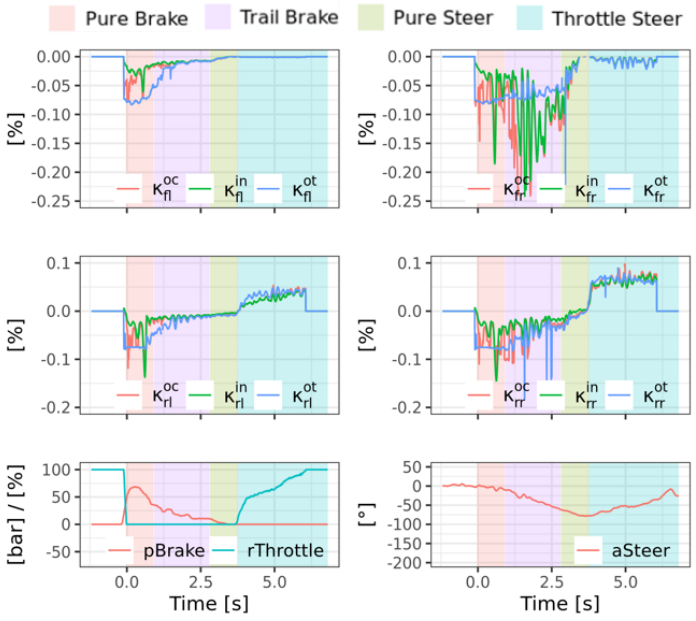
Comparing the Init state to the optTire state leads to insights how the vehicle is handled at the dynamic limit. We look at the initial and optimised slip ratios and slip angles of the tires.

4.1.1. Slip ratio κ

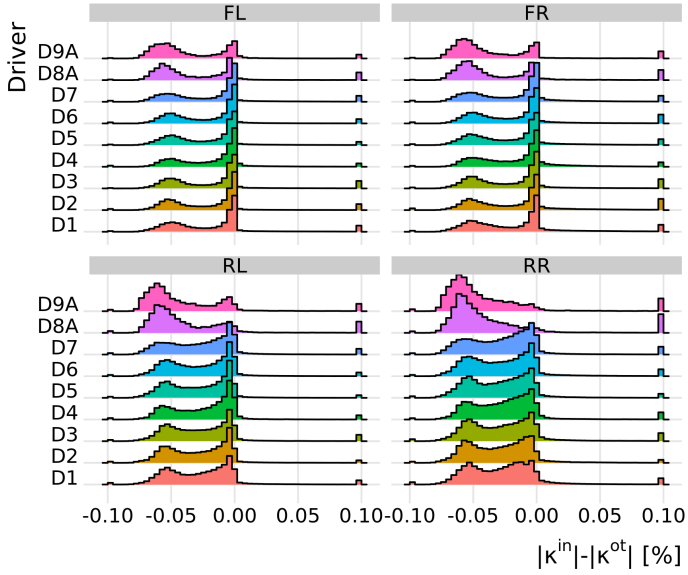
Figure 7a shows that the slip ratio in the optCog state κ^{oc} changes with a higher frequency in the Pure Brake zone than the Init state κ^{in}. The optTire state κ^{ot} which depicts the optimum slip ratio for each tire provides a reference. This optimum cannot be reached for all tires simultaneously, therefore the optCog optimiser has to make trade-offs by alternating the tires that reach the optimum. Figure 7b shows the distribution of slip ratio differences from the Init to the optTire state per tire. It seems that all drivers are very careful not to exceed the optimal value for κ, since that would lead quickly to a so called 'tire lock-up' in reality. That means the tire is no longer rotating while the vehicle is still moving and just rubbing over the road surface. A tire lock-up not only decreases the braking acceleration but also causes significant tire wear due to the high relative velocities, which in turn can significantly decrease performance for the following laps. For comparison the amateur drivers are shown as well. The center of the distributions is further away from the optimum both on the front and on the rear axle. We conclude that the amateur drivers are more cautious and cannot reach the optimum as well as the the professional drivers.

4.1.2. Slip angle α

Figure 8 gives a similar overview for the slip angle α. Figure 8a shows an example in the time domain. For the front axle (the two topmost plots) the Init and optCog state are close to each other, on the rear axle seems to be a larger gap. Over the complete data set the histograms in Figure 8b draw a similar picture. Instead of left and right the panel is split into inner and outer tire to make the analysis independent of a specific race track. What is more, during a cornering manoeuvre the outer tires have a higher normal force due to load transfer.
All professional drivers exceed the optimal slip angle α^{ot} at the front axle most of the time. For the outer front the distribution is bimodal for most drivers with a maximum at approx. $-2°$ and $1.5°$. Interestingly, on the inner front there is a more pronounced maximum a $0°$. On the outer rear all drivers clearly avoid slip angles higher than the optimum, resulting in a peak at $-2°$. The distribution on the inner rear has a wider range and reaches slightly in the positive values. The explanation for not exceeding the optimum on the outer rear axle is stability. Loosing grip on the rear axle would lead to an unstable oversteer and since the outer rear provides most of the grip it is more



a) Exemplary overview about κ in the time domain for the Init, optCog and optTire state.



b) κ difference distribution between the Init and optTire state for the complete data set over the four tires and drivers. Negative values indicate that the absolute of κ^{in} is smaller than the absolute of κ^{ot}.

Figure 7: The histograms (bottom plot) show the drivers very rarely exceed the optimal Slip Ratio κ. The top plot shows such rare occasion for the front right wheel.

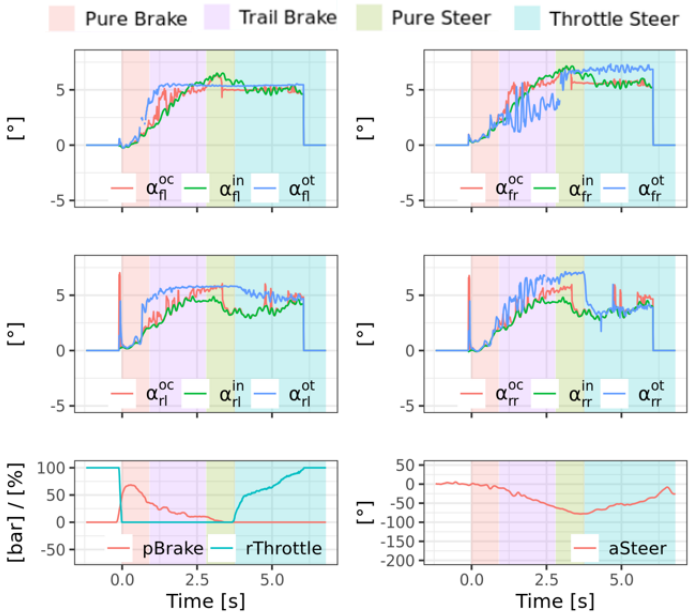
important to not exceed the optimum there than on the inner rear. On the front however, the drivers intentionally drive at higher slip angles than would be optimal because the generated lateral force stays relatively constant from the optimum towards higher slip angles but has a steeper slope from small values to the optimum. To better control the vehicle and anticipating it's reaction, the drivers stay in the more constant region above the optimum on purpose.
Between the professional drivers, some differences can be observed. On the outer and inner front tire, Driver D5 has a more unimodal distribution than the rest. On the inner rear tire, the same holds for Driver D4. The amateur drivers which are included as a reference have a distinctly different distribution. On the front, they have smaller slip angles than the optimum in general, however, instances where they have much higher slip angles than the optimum are also more frequent than for the professional drivers. On the rear axle the situation is similar. Analogical to the slip ratio, the amateur drivers are more cautious not to exceed the optimal slip angles.

4.2. optCog optimisation

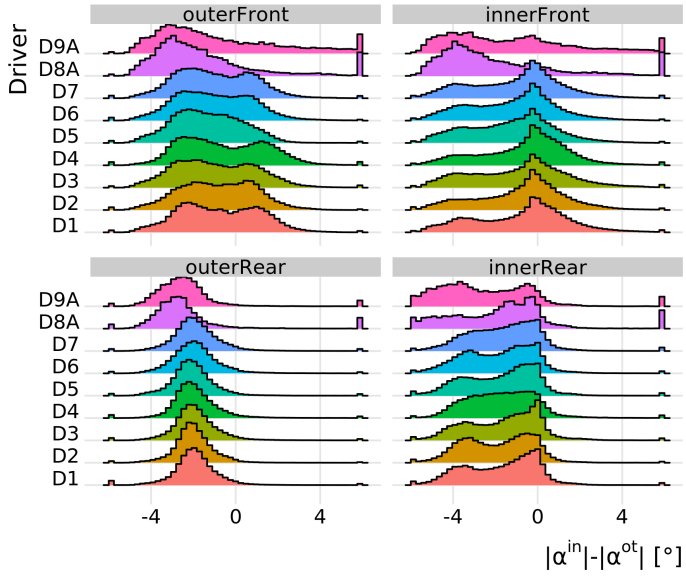
Figure 9a shows an exemplary overview of the acceleration from the optCog optimiser. It is close to the Init acceleration in the phases Pure Steer and Throttle Steer. For Trail Brake, the difference is slightly larger and for Pure Brake the optCog acceleration is significantly higher. The different control states are indicated by the coloured background.
A common visualization method in motorsport for accelerations is the 'GG-Diagram'; Figure 9b depicts the acceleration in x- and y-direction. It allows an understanding of the physical limits of the vehicle [1], assuming it was driven on the dynamic limit. The shape results from the frictional properties of the tires and their kinematic relations to each other (aerodynamic effects like downforce play a role as well). The symmetry of the ellipse is broken for acceleration and deceleration since the acceleration of the vehicle is not always limited by tire grip but also the engine power. In contrast, the brakes are designed to exert enough torque to use the full friction potential.
The comparison between the Init and optCog state shows large differences under Pure Brake (Decelerate) and slight differences under Trail Brake (between Decelerate and Right or Left). The other areas match closely.
We expect two factors to be responsible for the unrealistic high braking accelerations of the optCog state. First, the optimiser could directly control the tire slip ratio κ with the stated torque constraints. Since the optimiser has no information in the temporal domain, it leads to the high frequency changes in κ which could not be achieved in reality. Brake system compliance is also not considered due to this approach. Second, the drivers leave a margin to the optimal tire slip ratio to avoid lock-ups as discussed in Section 4.1.1.

4.3. Scores evaluation

Figure 10 shows an overview of the scores and the corresponding predictions in the time domain as well the distributions for the complete data set. As analysed previously, the ratio between the Init and the optCog acceleration S_{handling} is smaller for Pure Brake and Trail brake.

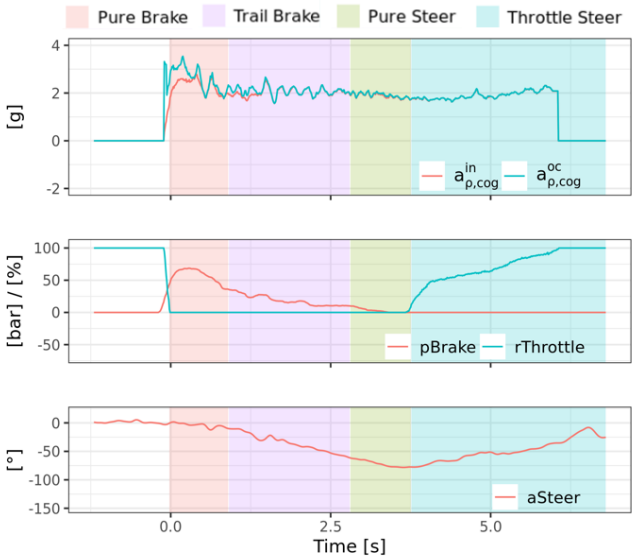


a) Exemplary overview about α in the time domain for the Init, optCog and optTire state.

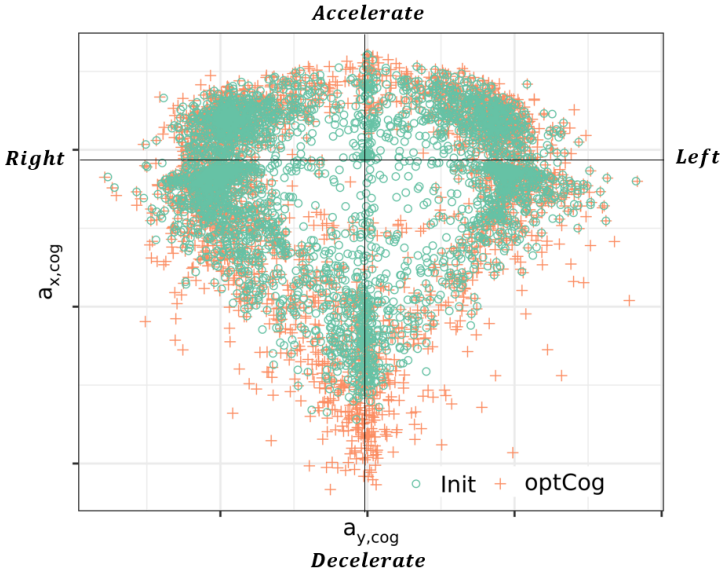


b) Distribution of slip angle differences between the Init and optTire state over the tires and drivers for all sections where $|gLat| \geq 1.5g$. Negative values indicate that the absolute of α^{in} is smaller than the absolute of α^{ot}. The panel is split into outer and inner tire instead of left and right tire to make it track independent.

Figure 8: Both panels show that the drivers often exceed the optimal slip angle α on the front axle, while usually staying below the limit at the rear axle. Especially on the outer rear axle, the drivers avoid overshooting the optimum. Differences between the professional and amateur drivers are clearly visible.



a) Exemplary overview about the accelerations from the Init and optCog state in the time domain as well as the brake, throttle and steering inputs from the driver. The background is coloured with respect to the defined control states.



b) 'GG-Diagram' of the accelerations in the xy-plane for the Init and optCog state. Under pure braking (decelerate) there is a significant difference between the two states.

Figure 9: optCog versus Init state accelerations.

Figure 10 b shows the differences given the control state. S_{handling} is spread much wider under Pure Brake than for the other three control states. What is more, the center of the distribution is shifted towards the left. For S_{tot} the situation is similar only that for Pure Brake 100% are almost never reached and that the Trail Brake score is skewed to the left.

This difference makes the control states, which were originally only defined to simplify the analysis for the drivers, necessary to compare different track sectors to each other. For example a track with more Pure Brake sections would lead to lower overall scores in comparison to a track with fewer of such sections. However, by analysing the scores for each control state individually, this will be compensated, resulting in a track independent benchmark. This is a valuable tool for engineers and race drivers which would not be possible without the presented methods.

4.4. Driving style evaluations

We provide an exemplary evaluation of the motorsport dataset to show how the presented methods are used and to give an insight into the differences between professional race drivers when controlling a vehicle at its dynamic limit.

4.4.1. Traditional lap-based metrics

It showed that the most useful representation are boxplots depicting certain characteristics from the distribution of scores. Of interest are the first quartile, the median and the third quartile, in other words the 25, 50 and 75% quantile. At first, traditional metrics are compared in Figure 11a on a per-lap basis. The lap time t_{lap} is probably the most important criteria to evaluate performance, however it provides no insights on how it is achieved. Closely related are the average velocity v_{avg} and the lap distance s_{lap}. Additionally, the integral over the absolute curvature c_{sum} which is obtained from the trajectory, is shown.

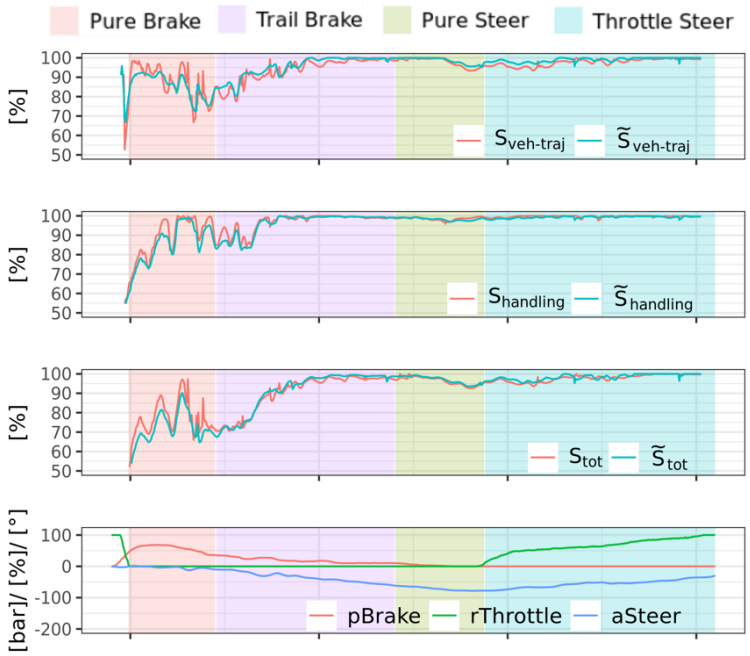
Looking at the medians, Driver D7 achieved the best laptimes, followed by driver D6. However, the variance is much higher for D7 according to the high spread of the box and the whiskers. This example shows already that the question 'which driver is the best' cannot be answered in general but depends on the circumstances. Differences are also present in s_{lap}. Driver D2 and D5 chose overall a longer driving line than the rest. The average speed results from lap time and lap distance naturally.

Although powerful, the disadvantage of these set of metrics is twofold. First, the most important metric t_{lap} can be used on a lap basis only. It is possible to use sector times by dividing the tracks in multiple parts, however, there is a limit on how short they can reasonably be. Second, these metrics do not always show where and why lap time differences occur.

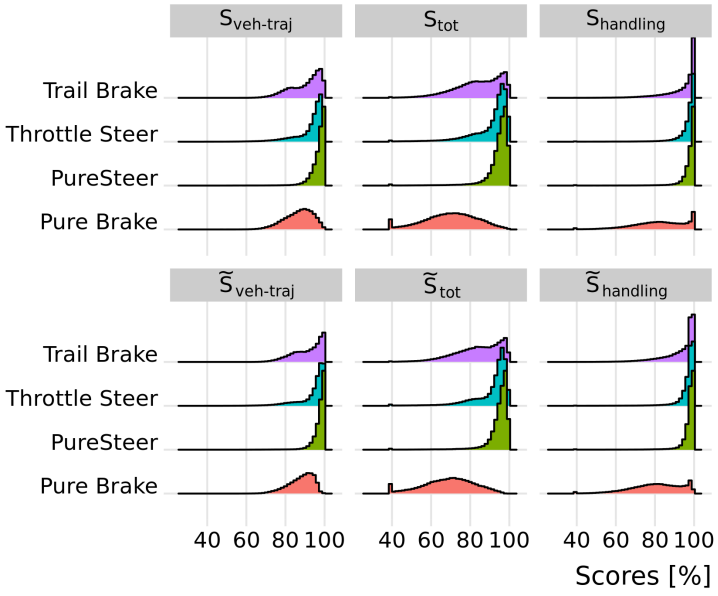
4.4.2. Professional race drivers

We show a visualization that can be used for a single corner, but also for a data set spanning multiple tracks as presented here. Figure 12 depicts the scores for pure brake and pure steer.

In the following we exemplary compare the drivers D5 and D6. Under pure braking in Figure 12a, D6 has a higher total score S_{tot} (Remark 1). We see that the difference arises because of a higher handling score S_{handling}, i.e. D6 is able to take the vehicle

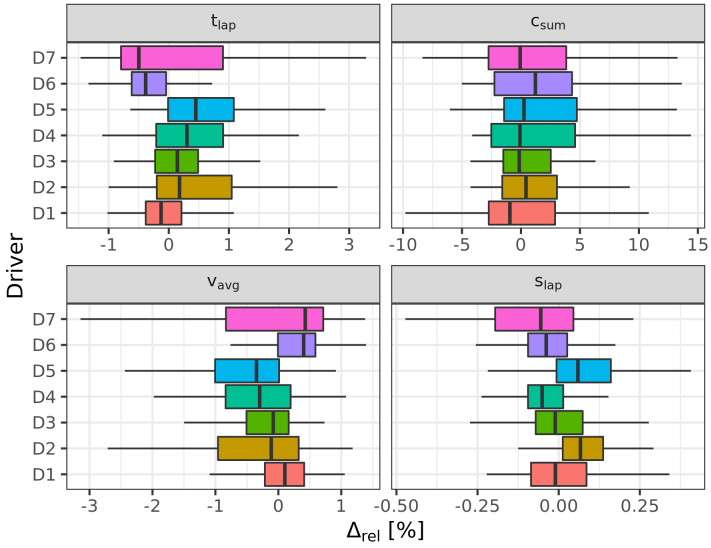


a) Exemplary overview about the defined scores and the machine learning predictions in the time domain.

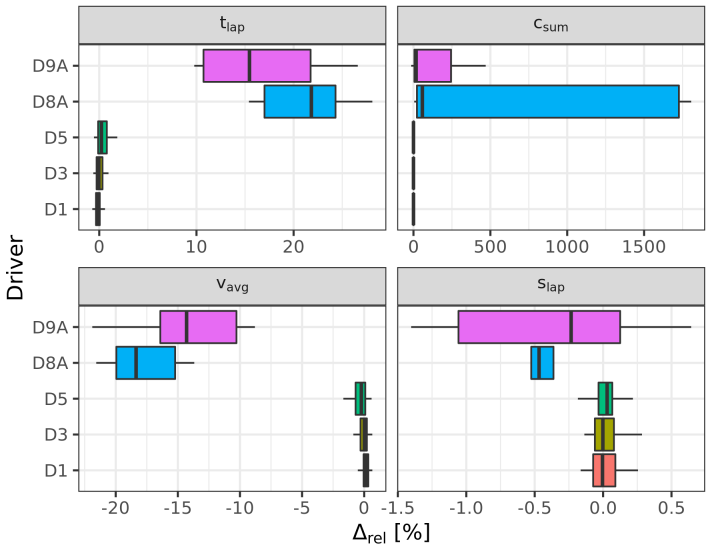


b) Scores overview for the complete data set over the control states. Scores smaller than 40% are grouped in the leftmost bin. Pure Brake and Trail Brake have a higher density in the lower scores.

Figure 10: Under braking the distribution of all scores and especially S_{handling} is skewed towards smaller values.



a) Professional drivers



b) Amateur versus professional drivers

Figure 11: Important metrics on a per-lap basis. All metrics are normed, the units are deviations from the median in %. *tLap* is the lap time, v_{avg} the average speed, c_{sum} the sum of the trajectory's curvature and *sLap* the lap distance. There are significant differences between professional and amateur drivers.

closer to its dynamic limit (Remark 2). Looking at $S_{\mathrm{veh-traj}}$, D5 has a slightly higher score, indicating that the optimised vehicle state is closer to the ideal tire state. To sum up, the higher $S_{\mathrm{veh-traj}}$ score cannot compensate the lower S_{handling} score.
Under pure steer D5 has a lower S_{tot} score, as shown in Figure 12b (Remark 3). Contrary to the difference in pure brake, the difference originates from the $S_{\mathrm{veh-traj}}$ score (Remark 4), i.e. D5 has a less advantageous vehicle setup or driving line. The handling scores for both drivers are comparable.
In conclusion, D6 is overall better than D5 in pure brake and pure steer. The fact that D6 performed better than D5 in the analysed data set is supported by the better lap times and average speeds of D6 which are shown in Figure 11a. However, in contrast to the lap time difference, the score analysis of this work allows much more detailed conclusions: D5 has to improve the handling skills under pure brake or needs a vehicle setup that has a better driveability.

4.4.3. Amateur Drivers

The differences in all of these scores were subtle for the professional drivers, which is natural given that they have been training for years to achieve the maximal performance. To test our proposed method further and make it more interesting for a broader audience, we examine also amateur drivers with road car driving skills but no motorsport race experience. For that purpose, they drove in the same simulator environment as the professional drivers with a comparable vehicle setup on the track T2. In Figure 11b significant differences between the two classes can be observed. For the amateurs, the lap time t_{lap} is 10 to 30% higher and the average speed v_{avg} 10 to 20% slower. The lap distance s_{lap} is shorter on average, which is a consequence of the much lower speed, allowing smaller cornering radii. D9A achieved quicker lap times than D8A, however, D8A was more consistent, especially in lap distance. Unsurprisingly, significant differences in S_{tot} are observed. Comparing the other two scores, the main difference comes from S_{handling}. Since all drivers drove a comparable vehicle setup, the differences can be clearly attributed to the trajectory.
Instead of providing the diagrams for all control states we summarized the information in Figure 13b. The mean difference between the professional and amateur drivers is depicted for every control state. Most of the amateurs' performance is lost under braking. Almost all of that is due to a worse handling score. The amateur drivers are worse at controlling the vehicle and we observed that they did not exploit the aerodynamic abilities of the vehicle. Because of high downforce, it is possible to brake much more at high speeds than at lower speeds. The highest difference in $S_{\mathrm{veh-traj}}$ is observed for throttle steer. Since the vehicle setups are equal, the reason has to be a difference in driving line. What is more, the difference in S_{handling} is the second highest leading to the highest S_{tot} difference after pure brake.
To sum up, the professional drivers' driving line is superior to the amateurs. However, the difference is much larger for the handling score. Most of the overall difference in S_{tot} is a result of the much lower S_{handling} score and not so much $S_{\mathrm{veh-traj}}$. For the amateur drivers to improve they would need to practice vehicle handling to be able to drive a higher speed along their chosen trajectory.

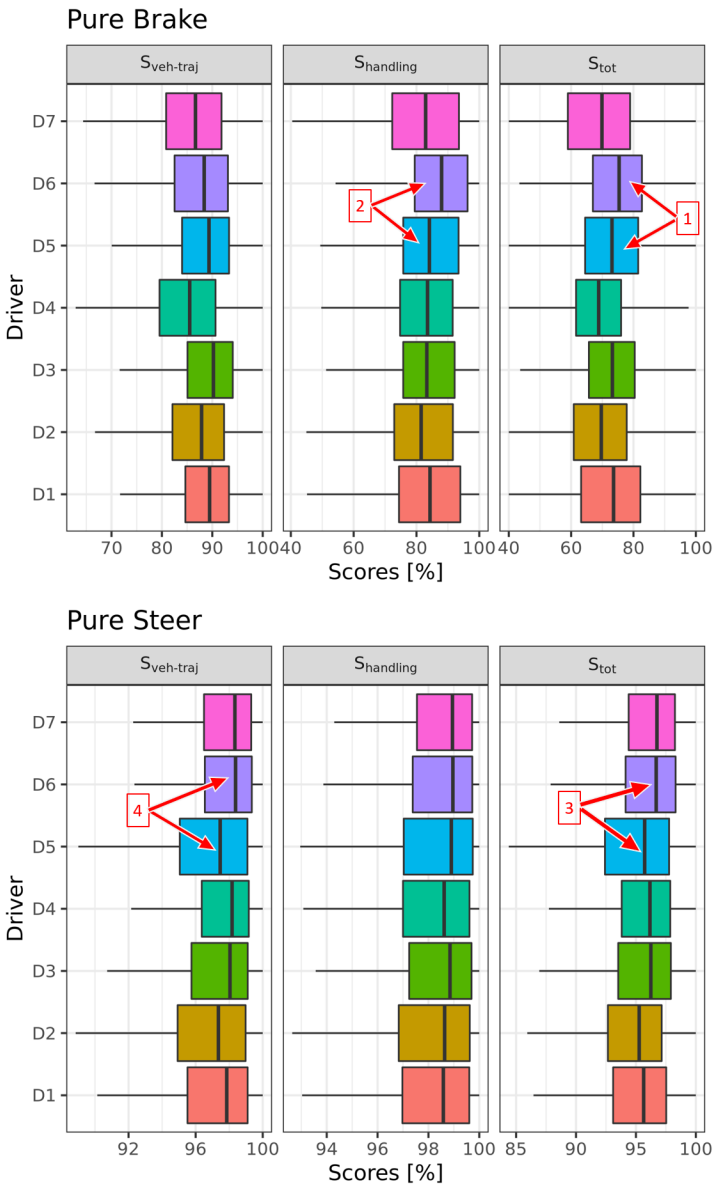
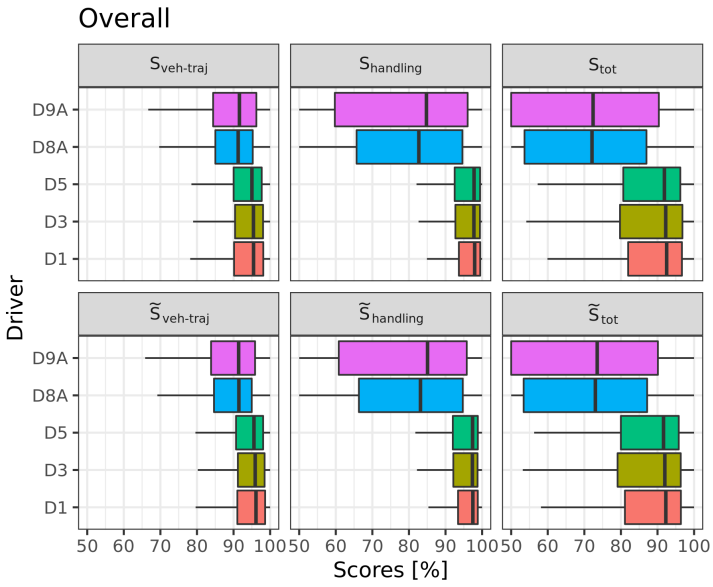
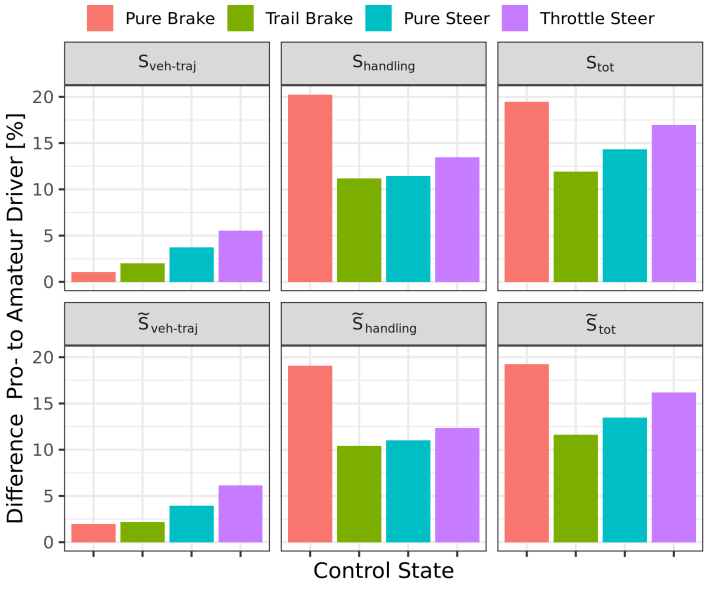


Figure 12: Exemplary score overview for the pure brake and pure steer states. The remarks show differences between the drivers D5 and D6.



a) Score overview for track T2 with amateur and professional drivers. In the first row are the score obtained by the optimisation procedure and in the second row the scores estimated by the machine learning predictor.



b) Difference between professional and amateur drivers for the control states. As expected the professional drivers have higher scores in all cases, therefore the difference is always positive. The difference in S_{tot} comes mainly from S_{handling}. In the second row are again the predictions of the machine learning model.

Figure 13: Professional versus amateur drivers.

4.5. Machine learning predictor evaluation

We already showed in Section 3.2.3 and Figure 6b that the predictions of the machine learning model have a RMSE in the area of 2% for S_{handling} and S_{tot} and around 3% for $S_{\text{veh}-\text{traj}}$ on the considered data set with the professional drivers. Consequently, the predictions are in good accordance with the dynamic limit optimisation method while greatly decreasing computation time. This is supported by Figure 10b where the score distributions for reference and prediction are very similar for the whole data set.
The prediction also shows good results for the amateurs who were not part of the training set and whose driving styles were very different compared to the training data. In this case the RMSE is approximately 3% for S_{handling} and S_{tot} and 5% for $S_{\text{veh}-\text{traj}}$. Comparing the optimisation scores in the first row of Figure 13b and the predictions in the second row they are very similar. Interpretation and analysis of both methods would lead to the same conclusion. What is more the difference between professional and amateur drivers is also very similar for both methods (Figure 13c).
In terms of computational speed, the machine learning predictor needed 12 seconds for inference (i.e. processing data through a trained neural network) on 1226 laps on a *NVIDIA®Tesla®V100* GPU, which is a specialized deep learning graphics card. High-end consumer graphic cards will achieve a performance in the same order of magnitude. In contrast, the optimisation methods needed over 68 hours for the same task on a computer with two 10-core *Intel®Xeon®Silver 4144* CPUs. Due to the different hardware and architecture (machine learning on the GPU, optimisation the CPU), the comparison might not be completely fair, however, the results show the massive improvement in computation time very clearly.
In conclusion, the robustness of the machine learning model and the low prediction error allows to replace the computational expensive optimisation methods with the machine learning predictor for our specific use case. Given the very fast computation time, a real time execution is also possible.

5. Conclusion

The presented methods showed their practical use for analysing drivers on a race track. However, it could be applied to all scenarios where the goal is to handle a vehicle at the limit. For road car driving, this can be the case for evasion manoeuvres or under slippery conditions. What is more, control systems for autonomous vehicles could be judged by the presented scores in a simulated environment and compared to professional drivers. However, what sets professional race drivers apart is their ability to not only handle a vehicles in a stable environment, but also in the real world under changing conditions. As a next step, we therefore propose a simulator study whereby the amount of grip is varied continuously. Having at hand the here presented driver evaluation methods, it could be investigated how the participants react to the grip changes and how long the adaptation time will be until the best possible performance is reached. We hope that further insight on how human experts achieve such high performance at controlling a vehicle at the limit helps the development of advanced autonomous control systems in the future.

Acknowledgement

This work was generously supported by BMW AG.

References

[1] J. C. Kegelman, Learning From Professional Race Car Drivers To Make Automated Vehicles Safer, Dissertation, Stanford University, 2018.

[2] E. Donges, Aspekte der aktiven sicherheit bei der führung von personenkraftwagen, Automobil Industrie 27 (1982) 183–190.

[3] C. C. Macadam, Understanding and modeling the human driver, Vehicle System Dynamics 40 (2003) 101–134. doi:10.1076/vesd.40.1.101.15875.

[4] L. Wörle, J. von Schleinitz, M. Graf, A. Eichberger, Driver detection from objective criteria describing the driving style of race car drivers, in: 2019 IEEE Intelligent Transportation Systems Conference (ITSC), 2019, pp. 1198–1203. doi:10.1109/ITSC.2019.8917325.

[5] L. Woerle, M. Graf, A. Eichberger, Objective metrics for control inputs of racecar drivers, Fisita F2018/F2018-VDY-050 (2018).

[6] J. C. Kegelman, L. K. Harbott, J. C. Gerdes, Insights into vehicle trajectories at the handling limits: analysing open data from race car drivers, Vehicle System Dynamics 55 (2017) 191–207. doi:10.1080/00423114.2016.1249893.

[7] J. von Schleinitz, L. Wörle, M. Graf, A. Schröder, W. Trutschnig, Analysis of race car drivers' pedal interactions by means of supervised learning, in: 2019 IEEE Intelligent Transportation Systems Conference (ITSC), 2019, pp. 4152–4157. doi:10.1109/ITSC.2019.8917120.

[8] J. Segers, Analysis Techniques for Racecar Data Acquisition, R.: Society of Automotive Engineers, SAE International, 2014. URL: https://books.google.de/books?id=C6FengEACAAJ.

[9] S. Löckel, J. Peters, P. van Vliet, A probabilistic framework for imitating human race driver behavior, IEEE Robotics and Automation Letters 5 (2020) 2086–2093. URL: http://arxiv.org/pdf/2001.08255v2. doi:10.1109/LRA.2020.2970620.

[10] F. Goy, J. Wiedemann, T. Völkl, G. Delli Colli, J. Neubeck, W. Krantz, Development of objective criteria to assess the vehicle performance utilized by the driver in near-limit handling conditions of racecars, in: M. Bargende, H.-C. Reuss, J. Wiedemann (Eds.), 16. Internationales Stuttgarter Symposium, Proceedings, Springer Fachmedien Wiesbaden, Wiesbaden, 2016, pp. 1213–1231. doi:10.1007/978-3-658-13255-2{\textunderscore}90.

[11] L. Hermansdorfer, J. Betz, M. Lienkamp, Benchmarking of a software stack for autonomous racing against a professional human race driver, 20.05.2020. URL: http://arxiv.org/pdf/2005.10044v1.

[12] S. de Groot, J. de Winter, On the way to pole position: The effect of tire grip on learning to drive a racecar, in: 2011 IEEE International Conference on Systems, Man, and Cybernetics, 2011, pp. 133–138. doi:10.1109/ICSMC.2011.6083655.

[13] P. M. van Leeuwen, S. de Groot, R. Happee, J. C. F. de Winter, Differences between racing and non-racing drivers: A simulator study using eye-tracking, PLOS ONE 12 (2017) e0186871. doi:10.1371/journal.pone.0186871.

[14] T. Schwarzhuber, J. von Schleinitz, H. Geiser, M. Graf, A. Eichberger, Drivers' controlled stimuli in nonlinear vehicle dynamics driving simulation, in: Proceedings of the Driving Simulation Conference 2020, Driving Simulation Association, 2020, p. 45.

[15] A. Liu, S. Chang, Force feedback in a stationary driving simulator, in: 1995 IEEE International Conference on Systems, Man and Cybernetics. Intelligent ystems for the 21st Century, IEEE, 1995, pp. 1711–1716. doi:10.1109/ICSMC.1995.538021.

[16] D. Toffin, G. Reymond, A. Kemeny, J. Droulez, Influence of steering wheel torque feedback in a dynamic driving simulator, in: DSC North America 2003 Proceedings, 2003.

[17] G. Markkula, R. Romano, R. Waldram, O. Giles, C. Mole, R. Wilkie, Modelling visual-vestibular integration and behavioural adaptation in the driving simulator, Transportation Research Part F: Traffic Psychology and Behaviour 66 (2019) 310–323. doi:10.1016/j.trf.2019.07.018.

[18] T. Schwarzhuber, L. Wörle, M. Graf, A. Eichberger, Validity qunatification of driver-in-the-loop simulation in motorsport, Fisita F2020 (waiting for Publication) 2020 (2020).

[19] B. Heißing, M. Ersoy, S. Gies (Eds.), Fahrwerkhandbuch: Grundlagen, Fahrdynamik, Komponenten, Systeme, Mechatronik, Perspektiven. Mit 80 Tabellen, ATZ/MTZ-Fachbuch, 4., überarb. u. erg. aufl. ed., Springer Vieweg, Wiesbaden, 2013.

[20] H. B. Pacejka, E. Bakker, The magic formula tyre model, Vehicle System Dynamics 21 (1992) 1–18. doi:10.1080/00423119208969994.
[21] L. Wörle, Objective Criteria for the Driving Style of Race Car Drivers, Doctoral thesis, TU Graz, Graz, 2020.
[22] R. N. Jazar, Vehicle Dynamics, Springer International Publishing, Cham, 2017. doi:10.1007/978-3-319-53441-1.
[23] MathWorks, fmincon, 2020. URL: https://de.mathworks.com/help/optim/ug/fmincon.html.
[24] J. von Schleinitz, M. Graf, W. Trutschnig, A. Schröder, Vasp: An autoencoder-based approach for multivariate anomaly detection and robust time series prediction with application in motorsport (waiting for publication), Under Review in Engineering Applications of Artificial Intelligence 2021 (2021).
[25] R Development Core Team, R: A language and environment for statistical computing, 2008. URL: http://www.R-project.org.
[26] J. J. Allaire, F. Chollet, keras: R interface to 'keras', 2018. URL: https://CRAN.R-project.org/package=keras.
[27] J. J. Allaire, Y. Tang, tensorflow: R interface to 'tensorflow', 2018. URL: https://CRAN.R-project.org/package=tensorflow.
[28] S. Hochreiter, J. Schmidhuber, Long short-term memory, Neural computation 9 (1997) 1735–1780. doi:10.1162/neco.1997.9.8.1735.
[29] G. van Houdt, C. Mosquera, G. Nápoles, A review on the long short-term memory model, Artificial Intelligence Review 53 (2020) 5929–5955. doi:10.1007/s10462-020-09838-1.
[30] D. P. Kingma, J. Ba, Adam: A method for stochastic optimization, 22.12.2014. URL: http://arxiv.org/pdf/1412.6980v9.